

UC Berkeley

UC Berkeley Previously Published Works

Title

Sulfur-doped graphene anchoring of ultrafine Au₂₅ nanoclusters for electrocatalysis

Permalink

<https://escholarship.org/uc/item/6bs6r3bt>

Journal

Nano Research, 14(10)

ISSN

1998-0124

Authors

Li, Mufan
Zhang, Bei
Cheng, Tao
[et al.](#)

Publication Date

2021-10-01

DOI

10.1007/s12274-021-3561-2

Peer reviewed

TABLE OF CONTENTS (TOC)

Sulfur-doped Graphene Anchoring of Ultrafine Au₂₅ Nanoclusters for Electrocatalysis

Mufan Li^{1,3,#}, Bei Zhang^{1,#}, Tao Cheng⁵, Sunmoon Yu^{2,3}, Sheena Louisia^{1,3}, Chubai Chen¹, Shouping Chen², Stefano Cestellos-Blanco², Miquel Salmeron³, William A. Goddard III⁵, Peidong Yang^{1,2,3,4*}

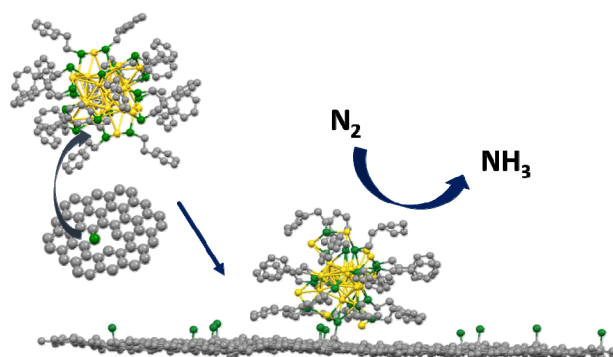
¹ Department of Chemistry, University of Berkeley, California 94720, United States

² Department of Materials Science and Engineering, University of Berkeley, California 94720, United States

³ Chemical Science Division, Lawrence Berkeley National Laboratory, Berkeley, California 94720, United States

⁴ Kavli Energy NanoScience Institute, Berkeley, California 94720, United States

⁵ Materials and Process Simulation Center, California Institute of Technology, Pasadena, California 91125, United States



The anchoring effect origin from sulfur-doped graphene enables a significantly enhanced stability of ultrafine Au nanoclusters during electrocatalytic nitrogen reduction.

Sulfur-doped Graphene Anchoring of Ultrafine Au₂₅ Nanoclusters for Electrocatalysis

Mufan Li^{1,3,#}, Bei Zhang^{1,#}, Tao Cheng⁵, Sunmoon Yu^{2,3}, Sheena Louisia^{1,3}, Chubai Chen¹, Shouping Chen², Stefano Cestellos-Blanco², Miquel Salmeron³, William A. Goddard III⁵, Peidong Yang^{1,2,3,4*} (✉)

¹ Department of Chemistry, University of Berkeley, California 94720, United States

² Department of Materials Science and Engineering, University of Berkeley, California 94720, United States

³ Chemical Science Division, Lawrence Berkeley National Laboratory, Berkeley, California 94720, United States

⁴ Kavli Energy NanoScience Institute, Berkeley, California 94720, United States

⁵ Materials and Process Simulation Center, California Institute of Technology, Pasadena, California 91125, United States

Received: day month year / Revised: day month year / Accepted: day month year (automatically inserted by the publisher)

©The Author(s) 2010. This article is published with open access at Springerlink.com

ABSTRACT

The biggest challenge of exploring the catalytic properties of under-coordinated nanoclusters is the issue of stability. We demonstrate herein that chemical dopants on sulfur-doped graphene (S-G) can be utilized to stabilize ultrafine (sub-2 nm) Au₂₅(PET)₁₈ clusters to enable stable nitrogen reduction reaction (NRR) without significant structural degradation. The Au₂₅@S-G exhibits an ammonia yield rate of 27.5 μg NH₃ mg_{Au}⁻¹h⁻¹ at -0.5 V with faradic efficiency of 2.3%. More importantly, the anchored clusters preserve ~80% NRR activity after four days of continuous operation, a significant improvement over the 15% remaining ammonia production rate for clusters loaded on undoped graphene tested under the same conditions. Isotope labeling experiments confirmed the ammonia was a direct reaction product of N₂ feeding gas instead of other chemical contaminations. *Ex-situ* X-ray photoelectron spectroscopy and X-ray absorption near-edge spectroscopy of post-reaction catalysts reveal that the sulfur dopant plays a critical role in stabilizing the chemical state and coordination environment of Au atoms in clusters. Further ReaxFF molecular dynamics (RMD) simulation confirmed the strong interaction between Au NCs and S-G. This substrate-anchoring process could serve as an effective strategy to study ultrafine nanoclusters' electrocatalytic behavior while minimizing the destruction of the under-coordinated surface motif under harsh electrochemical reaction conditions.

KEYWORDS

Gold nanoclusters, sulfur-doped graphene, nitrogen reduction reaction, electrocatalysis, anchoring effect.

1 Introduction

The discrete electronic structure of small Nanoclusters (from 3~40 atoms) can lead to unique properties chemical and spectroscopic properties [1] [2] [3] [4]. Moreover, because of the under-coordinated surface they can display unique chemisorption behaviors compared with conventional large nanoparticle systems (>2 nm diameter) [5]. Thus the ultrafine (from sub-nanometer to ~2 nm) nanoclusters (NCs) have attracted growing interest for applications to such catalytic reactions, as selective hydrogenation [6], carbon dioxide reduction [7] [8, 9], and carbon monoxide oxidation [10]. However, the significant surface under-coordinating nature of NCs tends to induce the sintering and aggregation of the clusters with formation of larger particles during reaction, considerably altering the experimental size-reactivity relationship. Hence, a crucial challenge to exploit the intrinsic catalytic properties of NCs [11] is to achieve cluster stability.

Extensive studies have demonstrated that porous materials such as metal-organic framework (MOF) [12] [13] [14] and zeolite materials [15] can effectively interact and confine metallic clusters having just a few atoms. However, the low conductivity of these carrier materials prevents their use as electrochemical substrates. Moreover, for electrocatalytic systems Ostwald ripening can cause severe agglomeration and destruction of the NCs. Thus, an ideal substrate that can stabilize under-coordinated nanoclusters in a harsh electrocatalysis environment should feature two critical characteristics:

- 1) good electrical conductivity that allows the electron transfer process;
- 2) strong anchoring capability to maintain the overall structure of ultrafine NCs.

It is well-established that Au forms relatively strong bond with sulfur atoms [16] [17]. Herein, we use sulfur-doped graphene (S-G) to demonstrate a dopant-anchoring strategy that can effectively stabilize the ultrafine $\text{Au}_{25}(\text{PET})_{18}$ cluster (abbreviated as Au_{25} for simplicity) for long term

electrocatalysis. The $\text{Au}_{25}@\text{S-G}$ exhibits remarkable stability for the nitrogen reduction reaction (NRR) with a superior ammonia production rate. *Ex-situ* structural characterizations confirmed that the morphology and chemical state of the ultrafine Au_{25} NCs are well maintained.

2 Experimental

2.1 Synthesis and isolation of $\text{Au}_{25}(\text{PET})_{18}$

Neutral $\text{Au}_{25}(\text{PET})_{18}$ nanocluster has been prepared by a modified method from a previously reported protocol [18]. $\text{HAuCl}_4 \cdot 3\text{H}_2\text{O}$ (19.7 mg, 0.05 mmol) and TOAB (32.8 mg, 0.06 mmol) were dissolved in a round bottom flask with 5 mL of tetrahydrofuran. The solution was vigorously stirred for 15 min to form a dark red solution. Phenylethanethiol (34.5 mg, 0.25 mmol) was then added to the solution. A transparent solution was obtained after 30 min. NaBH_4 (18.9 mg, 0.5 mmol) was dissolved in 1 mL ice-cold water and added immediately to the reaction mixture. The reaction was stopped after 24 h. The crude sample was precipitated by a large excessive of ice-cold water and washed with methanol 3 times to remove unreacted precursors and free TOAB. The crude sample was passed through a silica column and subsequent size-exclusion column to yield pure neutral $\text{Au}_{25}(\text{PET})_{18}$ nanocluster. The purity of the sample is confirmed by UV-vis, ESI-MS analysis, and ^1H NMR. The UV-vis spectrum of $\text{Au}_{25}(\text{PET})_{18}$ nanocluster shows the characteristic absorption at 402 nm, 459 nm, 639 nm, and 693 nm. ^1H NMR spectra of both TOAB and $\text{Au}_{25}(\text{PET})_{18}$ were recorded. The NMR peaks of $\text{Au}_{25}(\text{PET})_{18}$ are consistent with the reported spectrum, which differs from in $[\text{Au}_{25}(\text{PET})_{18}] \cdot \text{TOAB}^+$.¹ The peaks of TOAB at 3.56(t), 2.41(s), 1.73(s), and 1.14 (d) were not detected in $\text{Au}_{25}(\text{PET})_{18}$, confirming the complete removal of TOAB in $\text{Au}_{25}(\text{PET})_{18}$.

2.2 Physical characterizations

Transmission electron microscopy (TEM) was carried out using Hitachi H-7650. Inductively coupled plasma optical emission spectroscopy (ICP-OES) was tested using PerkinElmer Optima 7000 DV. XPS (Thermo Scientific K-alpha) measurement was conducted using an Al Ka source.

Address correspondence to p_yang@berkeley.edu

2.3 Catalyst loading and electrode preparation

Purified $\text{Au}_{25}(\text{PET})_{18}$ were dispersed in toluene solution and mixed with sulfur-doped graphene via vigorous stir (500 rpm) for 1 hour. The $\text{Au}_{25}\text{@S-G}$ were blow-dried by N_2 . For electrode preparation, $\text{Au}_{25}\text{@S-G}$ was dispersed in a mixture of ethanol and Nafion 117 solution (volume ratio of 100:1) with a concentration of $1 \text{ mg}_{\text{catalyst}} \text{ mL}^{-1}$ to form catalyst ink. The catalysts ink was drop cast on carbon paper ($0.5 \text{ cm} \times 2 \text{ cm}$) on both sides. The mass of loaded Au was measured by inductively coupled plasma - optical emission spectrometry (ICP-OES).

2.4 Electrochemical measurements

Electrochemical experiments

The nitrogen reduction reaction (NRR) experiments were carried out using a three-electrode Nafion membrane-separated H-cell on a BioLogic potentiostat system. A graphite rod and Ag/AgCl (3 M KCl) were used as counters electrode and a reference electrode, respectively. Note that both the Nafion membrane and graphite rod was pretreated in 5% H_2O_2 aqueous solution and ultrapure water at 80°C for 2 hours. 0.05 M H_2SO_4 was used as the electrolyte. Prior to NRR testing, the catalyst was activated by 20 potential cycles between -0.2 V to 0.2 V in Ar-saturated electrolyte for activation. To remove the trace NH_3 impurity, ultrapure N_2 gas (99.99%) was bubbled through H_2SO_4 (1 M) aqueous solution before fed into the electrolyte. The electrolyte is saturated with N_2 for 30 minutes ahead of NRR experiments. During the NRR experiment, a constant N_2 flow (20 sccm) was fed into the electrolyte at the cathode side. All potentials were calibrated into values versus reversible hydrogen electrode (RHE) via HER/HOR CV scan using two platinum wires as WE and CE.

2.5 Determination of ammonia concentration

Indophenol blue method was used to determine the ammonia concentration in the electrolyte. The

concentration of ammonia in the electrolyte was determined using the indophenol blue method with commercialized ammonia TNT830 vial test kit (Purchased from HACH). 5 mL electrolyte was added to the ammonia reagent vial. After inverting the cap, the vial was settled for 15 minutes before UV-Vis spectra was collected. The NH_3 production was indicated by the formation of indophenol blue, which was determined by the absorbance at 680 nm, with its concentration calibrated by a standard plot using a series of standard ammonium sulfate solutions. NMR measurements were done on a Bruker Avance 500 system with water suppression.

2.6 Isotope experiment

$^{15}\text{N}_2$ isotopic experiment was performed using the same setup with the only change to be the feeding gas was switch to $^{15}\text{N}_2$ gas. The cell was pre-purged with Ar for 30 min. The operation current at constant potential under $^{15}\text{N}_2$ was performed using the same potentiostat as above. The quantification of ammonia was accomplished by NMR of the post-reaction cathodic electrolyte.

3 Results and discussion

3.1 Synthesis and characterization of Au_{25}NCs and $\text{Au}_{25}\text{@S-G}$

We first synthesize $\text{Au}_{25}(\text{PET})_{18}$ nanoclusters via a conventional solution-phase method[18]. The synthesis protocol for NCs is illustrated in Figure 1a, with the experimental procedures detailed in SI Methods. The reaction time, temperature, and concentration of Au precursors were optimized to achieve good morphology and uniformity. The as-synthesized Au clusters were purified by passing through a silica column and subsequent size-exclusion column to yield pure neutral $\text{Au}_{25}(\text{PET})_{18}$ nanocluster. Ultraviolet-visible spectroscopy (UV-vis) and electrospray ionization mass spectrometry (ESI-MS) analysis were used to confirm the sample's purity. As shown in Figure 1b, UV-vis spectrum of $\text{Au}_{25}(\text{PET})_{18}$ nanocluster shows typical characteristic absorption peaks at 402 nm, 459 nm, 639 nm, and 693 nm (highlighted with the red dashes in Figure 1b), which agree with previous reported neutral $\text{Au}_{25}(\text{PET})_{18}$ results [18]. ESI-MS

results (Figure 1c) confirm that the purified nanoclusters are $\text{Au}_{25}(\text{PET})_{18}$ with atomic monodispersity, and the isotopic distribution patterns are consistent with simulated pattern of $\text{Au}_{25}(\text{PET})_{18}$ (Fig. S1). ^1H NMR spectra (Figure S2) confirmed the complete removal of TOAB in $\text{Au}_{25}(\text{PET})_{18}$.

To evaluate the stabilization capability of S-G, we used undoped graphene nanoplatelets (G) as a reference substrate for comparison. After purification of Au_{25} , the loading process was conducted by stir-mixing NCs and supporting materials in toluene at RT for 1 hour. Transmission electron microscopy (TEM) shows the overall size and uniformity of as-loaded Au_{25} . As shown in figure 1d, Au_{25} NCs were uniformly distributed on S-G with an ultrafine average size of 1.35 ± 0.45 nm based on statistical analysis (inset of Fig. 1d). In contrast, NCs loaded on graphene substrates show a significant trend toward aggregation. Nanoparticles with sizes ranging from 2~4 nm could be readily identified on the TEM image (Figure 1e). This aggregating phenomenon on graphene can be attributed to the lack of interacting species. $\text{Au}_{25}(\text{PET})_{18}$ can interact with the substrate only via π - π conjugation between the phenylethanethiol (PET) staple ligand and graphene.

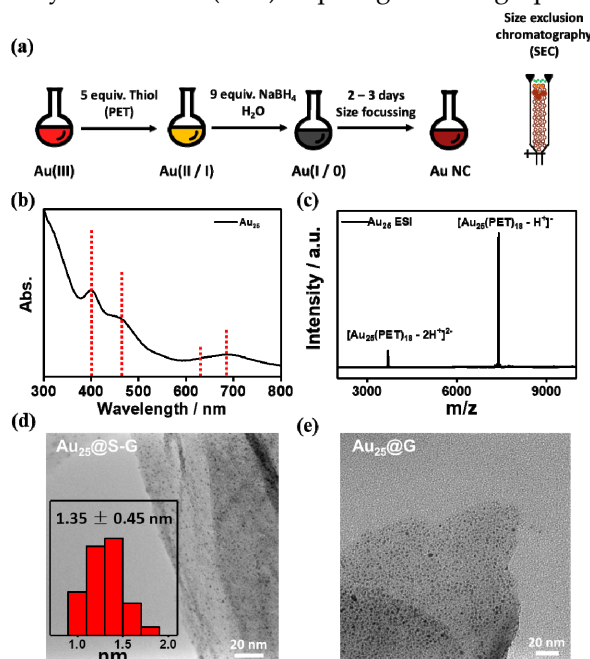


Figure 1. (a) Preparation procedure (b) UV-vis spectrum and (c) ESI-MS of as-synthesized $\text{Au}_{25}(\text{PET})_{18}$ clusters. Typical TEM images of $\text{Au}_{25}(\text{PET})_{18}$ clusters loaded on (d) sulfur-doped graphene and (e) graphene. The inset histogram of Fig. 1d shows the size distribution.

3.2 The electrocatalytic NRR tests of $\text{Au}_{25}@$ S-G and $\text{Au}_{25}@$ G

We performed the nitrogen reduction reaction in 0.05 M H_2SO_4 electrolyte to evaluate the electrocatalytic property and stability of the $\text{Au}_{25}@$ S-G composites. Au mass loading was determined to be to $11 \mu\text{g}/\text{cm}^2$ for both $\text{Au}_{25}@$ S-G and $\text{Au}_{25}@$ G (confirmed by inductively coupled plasma mass spectrometry). A graphite rod and an Ag/AgCl (WPI, 3M KCl) electrode were used as a counter electrode and reference electrode, respectively. The ammonia yield rate was determined by UV-Vis absorption spectra of the electrolyte stained with commercial indophenol indicator (TNT830) after 3h NRR operations under various electrochemical potentials. The concentration of NH_4^+ in the electrolyte was calibrated by a commercial standard ammonia solution. The standard plot shows a highly linear relationship between absorbance and concentration (Figure S3 a-c). As shown in figure 2a, $\text{Au}_{25}@$ S-G exhibits a peak NH_3 yield rate of $27.5 \mu\text{g NH}_3 \text{ mg}_{\text{Au}}^{-1} \text{h}^{-1}$ at -0.5 V with a faradic efficiency (FE) of 2.3%. This Au mass-normalized production rate is among the highest for previously reported Au-based NRR electrocatalysts [19] [20] [21]. When the operation potential was made more negative, both the ammonia production rate and the FE dropped dramatically due to the competing hydrogen evolution reaction (HER). As background reference, the NRR catalytic test with S-G alone shows negligible ammonia yield under the same electrochemical testing condition (Figure S4a and b). HAADF-STEM (Figure 2b and 2c) was used to monitor the morphology change between pristine Au_{25} and post-NRR Au_{25} . In this side-by-side comparison, the size and distribution of NCs on S-G remain mostly unchanged after 3 hours of NRR operation. The blurred substrate in the STEM image (Figure 2c) was induced by the addition of Nafion when preparing the electrode.

To detect trace amounts of ammonia, quantitative isotope measurement is needed to rule out potential contamination from the surrounding environment [22]. We conducted $^{15}\text{N}_2$ isotope labeling experiments to confirm that the source of nitrogen species in NH_4^+ generated comes from the N_2 feed gas (Figure S5a-c). We note that a set of tiny $^{14}\text{NH}_4^+$

background triplet peaks appear in the NMR spectra (Figure S5c). These peaks could be attributed to the 2-3% $^{14}\text{N}_2$ impurity in the $^{15}\text{N}_2$ isotope gas tank from the vendor.

Stability tests of $\text{Au}_{25}\text{@S-G}$ and $\text{Au}_{25}\text{@G}$ were conducted by chronoamperometry (CA) with operation potentials at -0.3 V vs. RHE. The tests were paused every 24h to analyze ammonia concentration in the catholyte, and the electrolyte was refreshed before resuming operation. The initial NRR activity of $\text{Au}_{25}\text{@S-G}$ was $9.5 \mu\text{g NH}_3 \text{ mg}_{\text{Au}}^{-1}\text{h}^{-1}$ at -0.3 V with a faradaic efficiency (FE) of 4.9%, while $\text{Au}_{25}\text{@G}$ exhibited $2.28 \mu\text{g NH}_3 \text{ mg}_{\text{Au}}^{-1}\text{h}^{-1}$ catalytic activity at -0.3 V with a faradaic efficiency (FE) of 1.85%. The ammonia production rate (R) was normalized by the initial rate (R_{initial}) at different times to compare the trend in stability. As shown in Figure 2d, The NH_3 yield rate for $\text{Au}_{25}\text{@S-G}$ drops ~4% per day for the first 96 hours. In contrast, a dropping rate of ~20% activity was observed for the $\text{Au}_{25}\text{@G}$ sample. TEM characterizations of post-test samples showed that S-G supported NCs (Figure 2e) maintained impressive dispersity and morphology even after 96 h catalytic operation. Whereas $\text{Au}_{25}\text{@G}$ (Figure 2f) leads to NCs suffering from severe agglomeration in the post durability test.

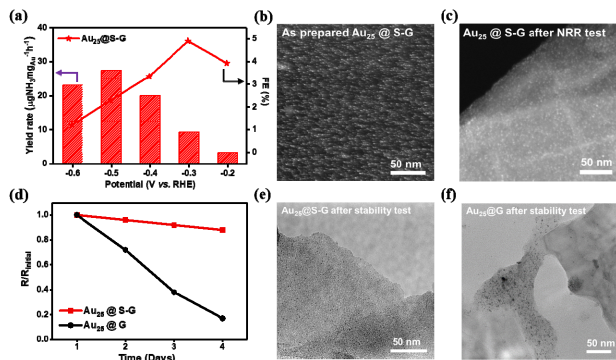


Figure 2. (a) Production rate of $\text{Au}_{25}\text{@S-G}$, faradaic efficiency of $\text{Au}_{25}\text{@S-G}$ at different potentials for 3 h tests. The star was referring to the FE, and the histogram represents the ammonia yield rate. HAADF-STEM image of the (b) as-prepared $\text{Au}_{25}\text{@S-G}$ and (c) $\text{Au}_{25}\text{@S-G}$ post electrolysis in 0.05 M H_2SO_4 at -0.3V for 3h. (d) Stability test of $\text{Au}_{25}\text{@S-G}$ and $\text{Au}_{25}\text{@G}$, respectively. TEM images of (E) $\text{Au}_{25}\text{@S-G}$ and (F) $\text{Au}_{25}\text{@G}$ post 96 hours NRR stability test.

3.3 The origin of the enhanced stability of $\text{Au}_{25}\text{@S-G}$ configuration

Ex-situ X-ray photoelectron spectroscopy (XPS) was used to probe the chemical state of Au species after interacting with the sulfur-doped substrate. The XPS

result for pristine Au_{25} NCs (Figure 3a) shows that the chemical state of Au in pristine clusters is predominately Au^0 , which is consistent with previous spectroscopy studies [23] [24]. After loading the NCs on S-G, the XPS of the $\text{Au}_{25}\text{@S-G}$ composite shows increasing Au^{x+} peaks with a binding energy of 86 eV and 89.6 eV for the Au 4f core-level region (labeled as a blue dot in Figure 3b), which we attribute to the interaction between sulfur-dopant on S-G with Au_{25} NCs. After conducting NRR at -0.3V for 3 h, the XPS for the post-reaction $\text{Au}_{25}\text{@S-G}$ shows a slightly increased Au^{x+} ratio (Figure 3c) compared with as-loaded NCs. This result indicates that the chemical state of the Au NCs is stable during catalytic operation, reflecting a strong interaction between sulfur dopant and NCs.

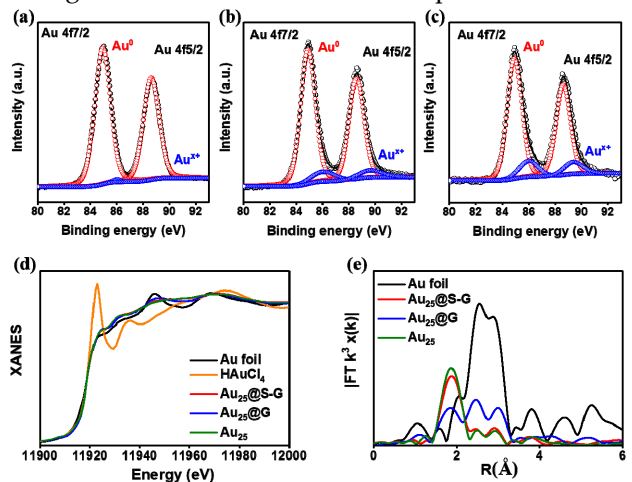


Figure 3. X-ray photoelectron spectroscopy of (a) as-synthesized $\text{Au}_{25}(\text{PET})_{18}$ clusters, (b) as-loaded $\text{Au}_{25}\text{@S-G}$ and (c) $\text{Au}_{25}\text{@S-G}$ post NRR test. (d) XAS and (e) Au L_3 edge FT-EXAFS of $\text{Au}_{25}\text{@S-G}$ and $\text{Au}_{25}\text{@G}$ post 3-hour NRR test at -0.3V vs. RHE, with Au foil and $\text{Au}_{25}(\text{PET})_{18}$ as the reference.

To investigate the interaction mechanism and to probe local Au atomistic and electronic structure, we conducted extended X-ray absorption fine structure (EXAFS) and X-ray absorption near-edge structure (XANES) measurements on $\text{Au}_{25}\text{@S-G}$ and $\text{Au}_{25}\text{@G}$ post 3h NRR tests at -0.3 V vs. RHE. The white line intensity probes the oxidation state of Au at the Au L-edge in XANES spectra. The Au XANES result shows that the white line intensities of both samples (Figure 3d) are close to that of an Au foil, indicating

that the average oxidation state of the NCs is close to a metallic state. The Au EXAFS (Figure 3e) fitting results shows an Au–Au bond length of 2.83 Å with CN = 1.1 (Table S1) for Au₂₅@S-G samples, which is in line with the value for pure Au₂₅ and for the predicted Au₁₃ icosahedral core group (Au–Au bond length 2.78, CN 1.44) in a previous structural study [25]. Moreover, both Au₂₅@S-G and Au₂₅ show a Au-S bond length of 2.32 Å with similar Au-S CN (1.8 of Au₂₅@S-G and 1.9 of Au₂₅). Combined with our XPS result, we conclude that the sulfur dopant on S-G partially replaces the thiol ligand to bind with outer Au atoms. This result also demonstrates that the Au₂₅@S-G can maintain the coordination characteristics of Au₂₅(PET)₁₈ even after the catalytic process.

In contrast, the EXAFS result for Au₂₅@G shows an Au–Au bond length 2.86 with CN of 4.1 post NRR, indicating that aggregation has caused Au₂₅ to lose cluster characteristics, getting closer to the bulk system. Additionally, comparing Au₂₅@S-G with pristine Au₂₅, the decreased Au-S coordination number (1.5 of Au₂₅@G *vs.* 1.8 of Au₂₅@S-G and 1.9 of Au₂₅) is plausible due to the ligand loss during sintering. This result shows that the monodispersed nanocluster without anchoring species on graphene aggregate during a dynamic electrocatalytic process.

To further reveal the sulfur-dopant role in stabilizing Au NCs, we carried out atomistic simulations using the reactive force field (ReaxFF). Based on the experimental results, we constructed two optimized models for computation study: 1) Au₂₅(PET)₁₈ on graphene (Figure 4a); 2) Au₂₅(PET)₁₈ on sulfur-doped graphene, with one ligand on the cluster replaced by a sulfur-dopant (Figure 4b). We calculated the binding energies of the two structures (Table S2), finding a binding energy of 2.23 eV for Au₂₅@G, and a binding energy of 7.11eV for Au₂₅@S-G. Therefore, the interaction of Au NCs with S-G is 4.88 eV stronger, consistent with experimental observations. More importantly, this stronger interaction will help prevent cluster aggregation. To prove this point, we carried out molecular dynamics simulations for Au₂₅ dimers on these surfaces, at 298K for 2 ns. The simulation results (Movie S1-2) show that in 2 ns of ReaxFF molecular dynamics (RMD) simulation,

sintering occurs for Au₂₅@G, but not for Au₂₅@S-G model(Figure S6). This shows that the enhanced binding can indeed play a role in stabilizing the Au NCs. These two observations are of the most importance in promoting catalysis performance and stability.

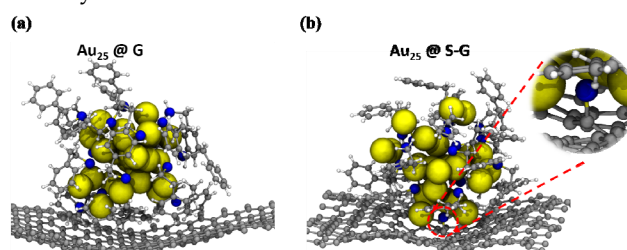


Figure 4. Results from 2ns reactive force field molecular dynamics (RMD) simulations followed by geometry optimization. Snapshots of (a) Au₂₅(PET)₁₈ on graphene and (b) Au₂₅(PET)₁₈ on sulfur-doped graphene, with one ligand on cluster replaced by sulfur-dopant after anchoring.

4 Conclusion

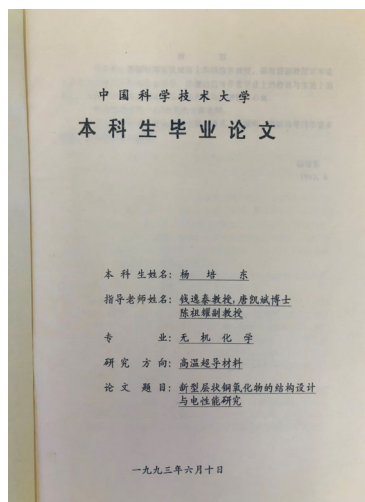
In conclusion, we successfully demonstrated that sulfur-doped graphene can stabilize ultrafine Au clusters for long term NRR electrocatalysis. The Au₂₅@S-G catalysts exhibit a high ammonia production rate of 27.5 μgNH₃ mg_{Au}⁻¹h⁻¹ with a faradic efficiency of 2.3 % at - 0.5 V. More importantly, the NCs maintain an 80% NRR yield rate after the 96 h stability test without morphology destruction. *Ex-situ* TEM and STEM characterizations highlighted the remarkable structural stability of the Au₂₅@S-G composite. XPS and EXAFS studies support the stabilized chemical state and coordination status of NCs after interacting with S-G. It would be interesting to extend this work, to consider substrates with other chemical dopants (e.g., N, P) to be utilized as an anchoring platform to probe the ultrafine NC intrinsic electrocatalytic behavior. This study may contribute to bridge the gap between conventional nanoparticles [20] [21] and molecular single atomic catalysts[19], to provide electrocatalytic mechanism insight about ultrafine nanoclusters.

Acknowledgements

This research was supported by Director, Office of Science, Office of Basic Energy Sciences, Chemical Sciences, Geosciences, & Biosciences Division, of the US Department of Energy under Contract DEAC02-05CH11231, FWP CH030201 (Catalysis

Research Program). The Advanced Light Source is supported by the Director, Office of Science, Office of Basic Energy Sciences, of the US Department of Energy under Contract DE-AC02-05CH11231. This work made use of the facilities at the NMR Facility, College of Chemistry, University of California, Berkeley. Inductively coupled plasma optical emission spectrometry was supported by the Microanalytical Facility, College of Chemistry, University of California, Berkeley. Part of this material (WAG, TC) is based on work performed by the Liquid Sunlight Alliance, which is supported by the U.S. Department of Energy, Office of Science, Office of Basic Energy Sciences, Fuels from Sunlight Hub under Award Number DE-SC0021266.

This work is dedicated to the occasion of 80th birthday for Prof. Yitai Qian. As the undergraduate advisor for one of the authors (PY), Prof. Qian has had profound impact on this author's career in the field of materials chemistry. PY would like to acknowledge the unconditional support, encouragement and guidance from Prof. Qian back in early 1990s. It was during that time PY started his journey in solid state chemistry, by working on high temperature cuprate superconductors and finishing his undergraduate thesis on this exciting topic. The title page of this thesis was attached here (dated June 10, 1993).



Electronic Supplementary Material: Supplementary material (further details of the EXAFS fitting, computational method, ¹H NMR for purified Au₂₅PET₁₈ clusters, UV-Vis calibration curves for

ammonia determination, isotope labeling NMR result, optimized coordinates for simulation model) is available in the online version of this article at http://dx.doi.org/10.1007/s12274-***.***.*** (automatically inserted by the publisher) and is accessible free of charge

References

- 1] Liu, L.; Corma, A. Metal catalysts for heterogeneous catalysis: From single atoms to nanoclusters and nanoparticles. *Chem Rev* **2018**, *118*, 4981-5079.
- 2] Liu, L.; Corma, A. Confining isolated atoms and clusters in crystalline porous materials for catalysis. *Nature Reviews Materials* **2020**.
- 3] Taylor, K. J.; Pettiette - Hall, C. L.; Cheshnovsky, O.; Smalley, R. E. Ultraviolet photoelectron spectra of coinage metal clusters. *The Journal of Chemical Physics* **1992**, *96*, 3319-3329.
- 4] <jp026731y.Pdf>.
- 5] Buceta, D.; Piñeiro, Y.; Vázquez-Vázquez, C.; Rivas, J.; López-Quintela, M. Metallic clusters: Theoretical background, properties and synthesis in microemulsions. *Catalysts* **2014**, *4*, 356-374.
- 6] Zhu, Y.; Qian, H.; Drake, B. A.; Jin, R. Atomically precise au₂₅(sr)₁₈ nanoparticles as catalysts for the selective hydrogenation of alpha,beta-unsaturated ketones and aldehydes. *Angew Chem Int Ed Engl* **2010**, *49*, 1295-8.
- 7] Zhang, H.; Liu, H.; Tian, Z.; Lu, D.; Yu, Y.; Cestellos-Blanco, S.; Sakimoto, K. K.; Yang, P. Bacteria photosensitized by intracellular gold nanoclusters for solar fuel production. *Nat Nanotechnol* **2018**, *13*, 900-905.
- 8] Austin, N.; Zhao, S.; McKone, J. R.; Jin, R.; Mpourmpakis, G. Elucidating the active sites for co₂ electroreduction on ligand-protected au₂₅ nanoclusters. *Catalysis Science & Technology* **2018**, *8*, 3795-3805.
- 9] Kauffman, D. R.; Thakkar, J.; Siva, R.; Matranga, C.; Ohodnicki, P. R.; Zeng, C.; Jin, R. Efficient electrochemical co₂ conversion powered by renewable energy. *ACS Appl Mater Interfaces* **2015**, *7*, 15626-32.
- 10] Kim, H. Y.; Lee, H. M.; Henkelman, G. Co oxidation mechanism on ceo(2)-supported au nanoparticles. *J Am Chem Soc* **2012**, *134*, 1560-70.

- 11] Zhang, B.; Chen, C.; Chuang, W.; Chen, S.; Yang, P. Size transformation of the $\text{Au}_{22}(\text{sg})_{18}$ nanocluster and its surface-sensitive kinetics. *J Am Chem Soc* **2020**, *142*, 11514-11520.
- 12] Vilhelmsen, L. B.; Walton, K. S.; Sholl, D. S. Structure and mobility of metal clusters in mofs: Au, Pd, and AuPd clusters in mof-74. *J Am Chem Soc* **2012**, *134*, 12807-16.
- 13] Dou, L.; Wu, S.; Chen, D.-L.; He, S.; Wang, F.-F.; Zhu, W. Structures and electronic properties of Au clusters encapsulated zif-8 and zif-90. *The Journal of Physical Chemistry C* **2018**, *122*, 8901-8909.
- 14] Li, J.; Wang, W.; Chen, W.; Gong, Q.; Luo, J.; Lin, R.; Xin, H.; Zhang, H.; Wang, D.; Peng, Q. et al. Sub-nm ruthenium cluster as an efficient and robust catalyst for decomposition and synthesis of ammonia: Break the "size shackles". *Nano Research* **2018**, *11*, 4774-4785.
- 15] Liu, L.; Diaz, U.; Arenal, R.; Agostini, G.; Concepcion, P.; Corma, A. Generation of subnanometric platinum with high stability during transformation of a 2d zeolite into 3d. *Nat Mater* **2017**, *16*, 132-138.
- 16] Hakkinen, H. The gold-sulfur interface at the nanoscale. *Nat Chem* **2012**, *4*, 443-55.
- 17] Burgi, T. Properties of the gold-sulphur interface: From self-assembled monolayers to clusters. *Nanoscale* **2015**, *7*, 15553-67.
- 18] Kauffman, D. R.; Alfonso, D.; Matranga, C.; Qian, H.; Jin, R. Experimental and computational investigation of Au_{25} clusters and CO_2 : A unique interaction and enhanced electrocatalytic activity. *J Am Chem Soc* **2012**, *134*, 10237-43.
- 19] Qiu, Y.; Peng, X.; Lu, F.; Mi, Y.; Zhuo, L.; Ren, J.; Liu, X.; Luo, J. Single-atom catalysts for the electrocatalytic reduction of nitrogen to ammonia under ambient conditions. *Chem Asian J* **2019**, *14*, 2770-2779.
- 20] Wang, H.; Yu, H.; Wang, Z.; Li, Y.; Xu, Y.; Li, X.; Xue, H.; Wang, L. Electrochemical fabrication of porous Au film on Ni foam for nitrogen reduction to ammonia. *Small* **2019**, *15*, e1804769.
- 21] Liu, D.; Zhang, G.; Ji, Q.; Zhang, Y.; Li, J. Synergistic electrocatalytic nitrogen reduction enabled by confinement of nanosized Au particles onto a two-dimensional Ti_3C_2 substrate. *ACS Appl Mater Interfaces* **2019**, *11*, 25758-25765.
- 22] Andersen, S. Z.; Colic, V.; Yang, S.; Schwalbe, J. A.; Nielander, A. C.; McEnaney, J. M.; Enemark-Rasmussen, K.; Baker, J. G.; Singh, A. R.; Rohr, B. A. et al. A rigorous electrochemical ammonia synthesis protocol with quantitative isotope measurements. *Nature* **2019**, *570*, 504-508.
- 23] Zhang, P. X-ray spectroscopy of gold-thiolate nanoclusters. *The Journal of Physical Chemistry C* **2014**, *118*, 25291-25299.
- 24] Mathew, A.; Varghese, E.; Choudhury, S.; Pal, S. K.; Pradeep, T. Efficient red luminescence from organic-soluble $\text{Au}_2(5)$ clusters by ligand structure modification. *Nanoscale* **2015**, *7*, 14305-15.
- 25] MacDonald, M. A.; Chevrier, D. M.; Zhang, P.; Qian, H.; Jin, R. The structure and bonding of $\text{Au}_{25}(\text{SR})_{18}$ nanoclusters from EXAFS: The interplay of metallic and molecular behavior. *The Journal of Physical Chemistry C* **2011**, *115*, 15282-15287.